Science Advances
AAAS

advances.sciencemag.org/cgi/content/full/6/13/eaay2497/DC1

Supplementary Materials for

High-frequency rectification via chiral Bloch electrons

Hiroki Isobe*, Su-Yang Xu, Liang Fu*

*Corresponding author. Email: hisobe@mit.edu (H.I.); liangfu@mit.edu (L.F.)

Published 27 March 2020, *Sci. Adv.* **6**, eaay2497 (2020)
DOI: 10.1126/sciadv.aay2497

This PDF file includes:

Supplementary Materials

Section S1. Semiclassical Boltzmann theory

We describe in detail the analysis of the semiclassical Boltzmann transport theory for the calculation of second-order response in noncentrosymmetric materials. We deal with spatially homogeneous systems and hence the electron distribution function $f(\boldsymbol{k}, \epsilon)$ does not depend on the spatial position, but on the wavevector $\boldsymbol{k}$ and the energy ϵ. We assume that the frequency of the external field ω is lower than the interband spacing, so that interband transitions are suppressed and negligible.

We calculate the distribution function in the presence of the external field by the semiclassical Boltzmann equation ($\hbar = 1$) (*28, 54*)

$$\frac{\partial f}{\partial t} + \dot{\boldsymbol{k}} \cdot \frac{\partial f}{\partial \boldsymbol{k}} = -C[f] \tag{S1}$$

The time derivative of the momentum is equal to the force felt by an electron wave packet: $\dot{\boldsymbol{k}} = \boldsymbol{F}$. We have an external electric field $\boldsymbol{E}(\omega)$, so that the force is $\boldsymbol{F} = -e\boldsymbol{E}(\omega)$. The collision integral $C[f]$ is given by (*28, 55*)

$$C[f] = \int_{\boldsymbol{k}'} [w_{\boldsymbol{k}'\boldsymbol{k}} f(\boldsymbol{k}, \epsilon) - w_{\boldsymbol{k}\boldsymbol{k}'} f(\boldsymbol{k}', \epsilon + \delta\epsilon_{\boldsymbol{k}'\boldsymbol{k}})] \tag{S2}$$

where $w_{\boldsymbol{k}'\boldsymbol{k}}$ is the scattering rate from a state with momentum $\boldsymbol{k}$ to one with $\boldsymbol{k}'$. In the following, we consider elastic scattering. Then, the scattering rate becomes

$$w_{\boldsymbol{k}'\boldsymbol{k}} = 2\pi |T_{\boldsymbol{k}'\boldsymbol{k}}| \delta(\epsilon_{\boldsymbol{k}'} - \epsilon_{\boldsymbol{k}}) \tag{S3}$$

with the scattering T matrix $T_{\boldsymbol{k}'\boldsymbol{k}}$. It is given by $T_{\boldsymbol{k}'\boldsymbol{k}} = \langle \boldsymbol{k}' | V | \psi_{\boldsymbol{k}} \rangle$, where $|\boldsymbol{k}\rangle$ is the eigenstate of H_0, the Hamiltonian in the clean limit, and $|\psi_{\boldsymbol{k}}\rangle$ is the eigenstate of $H_0 + V$, including the scattering V. $|\psi_{\boldsymbol{k}}\rangle$ can be obtained as the solution to the Lippman–Schwinger equation $|\psi_{\boldsymbol{k}}\rangle = |\boldsymbol{k}\rangle + (\epsilon_{\boldsymbol{k}} - H_0 + i\delta)^{-1} V |\psi_{\boldsymbol{k}}\rangle$. The energy shift is obtained as $\delta\epsilon_{\boldsymbol{k}'\boldsymbol{k}} = -\boldsymbol{F} \cdot \delta\boldsymbol{r}_{\boldsymbol{k}'\boldsymbol{k}}$ with the coordinate shift $\delta\boldsymbol{r}_{\boldsymbol{k}'\boldsymbol{k}} \approx (\boldsymbol{k}' - \boldsymbol{k}) \times \boldsymbol{\Omega}(\boldsymbol{k})$ for a weak scattering process with a small momentum change (*56*).

1.1 Scattering rate in noncentrosymmetric media

In noncentrosymmetric media, the probability of a scattering process $\boldsymbol{k} \rightarrow \boldsymbol{k}'$ and the inverted process $-\boldsymbol{k} \rightarrow -\boldsymbol{k}'$ can be different. For time-reversal systems, this imbalance is captured by decomposing the scattering rate into two parts

$$w_{\boldsymbol{k}\boldsymbol{k}'} = w^{(S)}_{\boldsymbol{k}\boldsymbol{k}'} + w^{(A)}_{\boldsymbol{k}\boldsymbol{k}'} \tag{S4}$$

where the symmetric and antisymmetric parts $w^{(S)}$ and $w^{(A)}$, respectively, is defined by

$$w^{(S)}_{\boldsymbol{k}\boldsymbol{k}'} = \frac{1}{2}(w_{\boldsymbol{k}\boldsymbol{k}'} + w_{\boldsymbol{k}'\boldsymbol{k}}), \quad w^{(A)}_{\boldsymbol{k}\boldsymbol{k}'} = \frac{1}{2}(w_{\boldsymbol{k}\boldsymbol{k}'} - w_{\boldsymbol{k}'\boldsymbol{k}}) \tag{S5}$$

When time reversal is preserved, the scattering rate satisfies the reversibility $w_{\boldsymbol{k}\boldsymbol{k}'} = w_{-\boldsymbol{k}',-\boldsymbol{k}}$, which leads to the relations

$$w^{(S)}_{\boldsymbol{k}'\boldsymbol{k}} = w^{(S)}_{-\boldsymbol{k},-\boldsymbol{k}'} = w^{(S)}_{\boldsymbol{k}\boldsymbol{k}'} \tag{S6}$$

$$w^{(A)}_{\boldsymbol{k}'\boldsymbol{k}} = -w^{(A)}_{-\boldsymbol{k},-\boldsymbol{k}'} = -w^{(A)}_{\boldsymbol{k}\boldsymbol{k}'} \tag{S7}$$

Those equalities do not hold in general when time reversal is broken since states at $\boldsymbol{k}$ and $-\boldsymbol{k}$ usually have different energies. The optical theorem for elastic scattering guarantees the relation

$$\int_{\boldsymbol{k}'} w^{(A)}_{\boldsymbol{k}\boldsymbol{k}'} = 0 \tag{S8}$$

When the elastic scattering is due to impurities, $w^{(S)}$ and $w^{(A)}$ are obtained to the lowest order in the impurity scattering potential by

$$w^{(S)}_{\boldsymbol{k}'\boldsymbol{k}} = 2\pi\langle|V_{\boldsymbol{k}'\boldsymbol{k}}|^2\rangle\delta(\epsilon_{\boldsymbol{k}'} - \epsilon_{\boldsymbol{k}}) \tag{S9}$$

$$w^{(A)}_{\boldsymbol{k}'\boldsymbol{k}} = -(2\pi)^2 \int_{\boldsymbol{q}} \mathrm{Im}\langle V_{\boldsymbol{k}'\boldsymbol{q}} V_{\boldsymbol{q}\boldsymbol{k}} V_{\boldsymbol{k}\boldsymbol{k}'}\rangle\delta(\epsilon_{\boldsymbol{k}} - \epsilon_{\boldsymbol{k}'})\delta(\epsilon_{\boldsymbol{k}'} - \epsilon_{\boldsymbol{q}}) \tag{S10}$$

where $\langle\ \rangle$ denotes the average over the impurity distribution and $V_{\boldsymbol{k}'\boldsymbol{k}}$ is the matrix element for the single impurity scattering. We can see that the symmetric part of the scattering rate is

obtained at the lowest order of the Born approximation, whereas the antisymmetric part is found at the next leading order. The detailed balance is broken when the antisymmetric part is finite.

Reference (*27*) reviews the photogalvanic effect in noncentrosymmetric materials, considering the asymmetry of scattering. The photovoltaic effect is studied with the Boltzmann equation and the antisymmetric component of the scattering rate $w^{(A)}_{\boldsymbol{k}'\boldsymbol{k}}$, similarly to our analysis. A difference can be found in the origin of finite $w_{\boldsymbol{k}'\boldsymbol{k}}$. In Ref. (*27*), the asymmetry is imposed on scattering potentials for impurity scattering, ionization, photoexcitation, and recombination. We note that the asymmetry of the scattering rate can be finite due to an asymmetric scattering potential and also a wavefunction of a noncentrosymmetric medium. For the latter case, a scattering potential does not need to be inversion asymmetric to have finite $w^{(A)}_{\boldsymbol{k}'\boldsymbol{k}}$, but even an isotropic scattering potential can generate $w^{(A)}_{\boldsymbol{k}'\boldsymbol{k}}$ through a wavefunction.

1.2 Formal solutions

The semiclassical Boltzmann equation S1 should be solved self-consistently to obtain the distribution function $f(\boldsymbol{k})$. A fully self-consistent solution is generally difficult to obtain; here we decompose the distribution function f as

$$f = f_0 + f^{\mathrm{scatt}} + f^{\mathrm{adist}} \tag{S11}$$

The first term f_0 is the distribution function in equilibrium, i.e., the Fermi–Dirac distribution. The second term f^{scatt} describes the scattering contribution without the Berry curvature and the last term f^{adist} is the anomalous distribution due to the Berry curvature and the energy shift $\delta\epsilon_{\boldsymbol{k}'\boldsymbol{k}}$. We further expand f^{scatt} and f^{adist} with respect to the electric field $\boldsymbol{E}(\omega)$ and the asymmetric part of the scattering rate $w^{(A)}$:

$$f^{\mathrm{scatt}}(\boldsymbol{k}) = \sum_{n\geq 1} f^{\mathrm{scatt}}_n(\boldsymbol{k}), \quad f^{\mathrm{scatt}}_n(\boldsymbol{k}) = \sum_{m\geq 0} f^{(m)}_n(\boldsymbol{k}) \tag{S12}$$

$$f^{\mathrm{adist}}(\boldsymbol{k}) = \sum_{n\geq 1} f^{\mathrm{adist}}_n(\boldsymbol{k}), \quad f^{\mathrm{adist}}_n(\boldsymbol{k}) = \sum_{m\geq 0} g^{(m)}_n(\boldsymbol{k}) \tag{S13}$$

The subscript n and the superscript m correspond to the orders of the electric field E and the antisymmetric scattering rate $w^{(A)}$, respectively. As we have seen in Eqs. S9 and S10, $w^{(A)}$ is smaller than $w^{(S)}$, so that we treat the former as a perturbation. Then, the Boltzmann equation is decomposed for each $f_n^{(m)}$ or $g_n^{(m)}$ to become

$$\frac{\partial f_1^{(0)}}{\partial t} - e\boldsymbol{E}\cdot\frac{\partial f_0}{\partial \boldsymbol{k}} = -\int_{\boldsymbol{k}'} w^{(S)}_{\boldsymbol{k}\boldsymbol{k}'}[f_1^{(0)}(\boldsymbol{k}) - f_1^{(0)}(\boldsymbol{k}')] \tag{S14}$$

$$\frac{\partial f_1^{(1)}}{\partial t} = -\int_{\boldsymbol{k}'} w^{(S)}_{\boldsymbol{k}\boldsymbol{k}'}[f_1^{(1)}(\boldsymbol{k}) - f_1^{(1)}(\boldsymbol{k}')] + \int_{\boldsymbol{k}'} w^{(A)}_{\boldsymbol{k}\boldsymbol{k}'} f_1^{(0)}(\boldsymbol{k}') \tag{S15}$$

$$\frac{\partial f_2^{(0)}}{\partial t} - e\boldsymbol{E}\cdot\frac{\partial f_1^{(0)}}{\partial \boldsymbol{k}} = -\int_{\boldsymbol{k}'} w^{(S)}_{\boldsymbol{k}\boldsymbol{k}'}[f_2^{(0)}(\boldsymbol{k}) - f_2^{(0)}(\boldsymbol{k}')] \tag{S16}$$

$$\frac{\partial f_2^{(1)}}{\partial t} - e\boldsymbol{E}\cdot\frac{\partial f_1^{(1)}}{\partial \boldsymbol{k}} = -\int_{\boldsymbol{k}'} w^{(S)}_{\boldsymbol{k}\boldsymbol{k}'}[f_2^{(1)}(\boldsymbol{k}) - f_2^{(1)}(\boldsymbol{k}')] + \int_{\boldsymbol{k}'} w^{(A)}_{\boldsymbol{k}\boldsymbol{k}'} f_2^{(0)}(\boldsymbol{k}') \tag{S17}$$

$$\frac{\partial g_1^{(0)}}{\partial t} = -\int_{\boldsymbol{k}'} w^{(S)}_{\boldsymbol{k}\boldsymbol{k}'}[g_1^{(0)}(\boldsymbol{k}) - g_1^{(0)}(\boldsymbol{k}')] + \int_{\boldsymbol{k}'} w^{(S)}_{\boldsymbol{k}\boldsymbol{k}'} f_0'(\boldsymbol{k}')(e\boldsymbol{E}\cdot\delta\boldsymbol{r}_{\boldsymbol{k}'\boldsymbol{k}}) \tag{S18}$$

$$\frac{\partial g_1^{(1)}}{\partial t} = -\int_{\boldsymbol{k}'} w^{(S)}_{\boldsymbol{k}\boldsymbol{k}'}[g_1^{(1)}(\boldsymbol{k}) - g_1^{(1)}(\boldsymbol{k}')] + \int_{\boldsymbol{k}'} w^{(A)}_{\boldsymbol{k}\boldsymbol{k}'} g_1^{(0)}(\boldsymbol{k}') + \int_{\boldsymbol{k}'} w^{(A)}_{\boldsymbol{k}\boldsymbol{k}'} f_0'(\boldsymbol{k}')(e\boldsymbol{E}\cdot\delta\boldsymbol{r}_{\boldsymbol{k}'\boldsymbol{k}}) \tag{S19}$$

$$\begin{aligned}&\frac{\partial g_2^{(0)}}{\partial t} - e\boldsymbol{E}\cdot\frac{\partial g_1^{(0)}}{\partial \boldsymbol{k}}\\ &= -\int_{\boldsymbol{k}'} w^{(S)}_{\boldsymbol{k}\boldsymbol{k}'}[g_2^{(0)}(\boldsymbol{k}) - g_2^{(0)}(\boldsymbol{k}')] + \int_{\boldsymbol{k}'} w^{(S)}_{\boldsymbol{k}\boldsymbol{k}'}[f_1'^{(0)}(\boldsymbol{k}') + g_1'^{(1)}(\boldsymbol{k}')](e\boldsymbol{E}\cdot\delta\boldsymbol{r}_{\boldsymbol{k}'\boldsymbol{k}})\\ &\quad + \frac{1}{2}\int_{\boldsymbol{k}'} w^{(S)}_{\boldsymbol{k}\boldsymbol{k}'} f_0''(\boldsymbol{k}')(e\boldsymbol{E}\cdot\delta\boldsymbol{r}_{\boldsymbol{k}'\boldsymbol{k}})^2\end{aligned} \tag{S20}$$

$$\begin{aligned}&\frac{\partial g_2^{(1)}}{\partial t} - e\boldsymbol{E}\cdot\frac{\partial g_1^{(1)}}{\partial \boldsymbol{k}}\\ &= -\int_{\boldsymbol{k}'} w^{(S)}_{\boldsymbol{k}\boldsymbol{k}'}[g_2^{(1)}(\boldsymbol{k}) - g_2^{(1)}(\boldsymbol{k}')] + \int_{\boldsymbol{k}'} w^{(S)}_{\boldsymbol{k}\boldsymbol{k}'}[f_1'^{(1)}(\boldsymbol{k}') + g_1'^{(1)}](e\boldsymbol{E}\cdot\delta\boldsymbol{r}_{\boldsymbol{k}'\boldsymbol{k}})\\ &\quad + \int_{\boldsymbol{k}'} w^{(A)}_{\boldsymbol{k}\boldsymbol{k}'} g_2^{(0)}(\boldsymbol{k}') + \int_{\boldsymbol{k}'} w^{(A)}_{\boldsymbol{k}\boldsymbol{k}'}[f_1'^{(0)}(\boldsymbol{k}') + g_1'^{(0)}](e\boldsymbol{E}\cdot\delta\boldsymbol{r}_{\boldsymbol{k}'\boldsymbol{k}}) + \frac{1}{2}\int_{\boldsymbol{k}'} w^{(A)}_{\boldsymbol{k}\boldsymbol{k}'} f_0''(\boldsymbol{k}')(e\boldsymbol{E}\cdot\delta\boldsymbol{r}_{\boldsymbol{k}'\boldsymbol{k}})^2\end{aligned} \tag{S21}$$

A prime symbol $'$ added to the distribution functions stands for the derivative with respect to the energy: $f'(\boldsymbol{k},\epsilon) = \partial_\epsilon f(\boldsymbol{k},\epsilon)$.

Each equation has to be solved self-consistently; however it is usually not easy. Here, we

solve a part of the collision integral involving $w^{(S)}$ self-consistently, while the other part with $w^{(A)}$ is treated as a perturbation. The collision integrals with $w^{(S)}$ define the scattering times $\tau_n^{(m)}$ and $\tau_n^{(m)}$ as follows

$$\int_{\boldsymbol{k}'} w^{(S)}_{\boldsymbol{k}\boldsymbol{k}'}[f_n^{(m)}(\boldsymbol{k}) - f_n^{(m)}(\boldsymbol{k}')] = \frac{1}{\tau_n^{(m)}} f_n^{(m)}(\boldsymbol{k}) \tag{S22}$$

$$\int_{\boldsymbol{k}'} w^{(S)}_{\boldsymbol{k}\boldsymbol{k}'}[g_n^{(m)}(\boldsymbol{k}) - g_n^{(m)}(\boldsymbol{k}')] = \frac{1}{\tau_n'^{(m)}} g_n^{(m)}(\boldsymbol{k}) \tag{S23}$$

If $\tau_n^{(m)}$ and $\tau_n'^{(m)}$ do not satisfy the self-consistency, one may regard the equations above as the definitions for the relaxation time approximation. We also note the notation of the scattering times τ_n and τ_n' used in the main text; they correspond to $\tau_n \equiv \tau_n^{(0)}$ and $\tau_n' \equiv \tau_n^{(1)}$.

We assume τ and τ' are independent of momentum $\boldsymbol{k}$ in solving the equations. Then, we obtain the formal solutions for the distribution functions $f_n^{(m)}$ and $g_n^{(m)}$. The second-order response contains different frequencies, 0 and $\pm 2\omega$. Since now we focus on rectification, i.e., zero-frequency response, we only write down the second-order solutions with $\omega = 0$. Now, we list below the formal solutions up to the second order in the electric field ($n \leq 2$) and to the first order in $w^{(A)}$ ($m \leq 1$)

$$f_1^{(0)}(\boldsymbol{k}, \omega) = \tau_{1\omega}^{(0)} e E_a \partial_{k_a} f_0(\boldsymbol{k}) \tag{S24}$$

$$f_1^{(1)}(\boldsymbol{k}, \omega) = \tau_{1\omega}^{(1)} \int_{\boldsymbol{k}'} w^{(A)}_{\boldsymbol{k}\boldsymbol{k}'} \tau_{1\omega}^{(0)} e E_a \partial_{k'_a} f_0(\boldsymbol{k}') \tag{S25}$$

$$f_2^{(0)}(\boldsymbol{k}, 0) = \tau_2^{(0)} e E_a^* \partial_{k_a} f_1^{(0)}(\boldsymbol{k}, \omega) + \text{c.c.} = \tau_2^{(0)} e E_a^* \partial_{k_a} \tau_{1\omega}^{(0)} e E_b \partial_{k_b} f_0(\boldsymbol{k}) + \text{c.c.} \tag{S26}$$

$$\begin{aligned} & f_2^{(1)}(\boldsymbol{k}, 0) \\ &= \tau_2^{(1)} e E_a^* \partial_{k_a} f_1^{(1)}(\boldsymbol{k}, \omega) + \text{c.c.} + \int_{\boldsymbol{k}'} w^{(A)}_{\boldsymbol{k}\boldsymbol{k}'} f_2^{(0)}(\boldsymbol{k}', 0) \\ &= \tau_2^{(1)} e E_a^* \partial_{k_a} \tau_{1\omega}^{(1)} \int_{\boldsymbol{k}'} w^{(A)}_{\boldsymbol{k}\boldsymbol{k}'} \tau_{1\omega}^{(0)} e E_b \partial_{k'_b} f_0(\boldsymbol{k}') + \tau_2^{(1)} \int_{\boldsymbol{k}'} w^{(A)}_{\boldsymbol{k}\boldsymbol{k}'} \tau_2^{(0)} e E_a^* \partial_{k'_a} \tau_{1\omega}^{(0)} e E_b \partial_{k'_b} f_0(\boldsymbol{k}') + \text{c.c.} \end{aligned} \tag{S27}$$

$$g_1^{(0)}(\boldsymbol{k}, \omega) = \tau_{1\omega}'^{(0)} \int_{\boldsymbol{k}'} w^{(S)}_{\boldsymbol{k}\boldsymbol{k}'} f_0'(\boldsymbol{k}') e E_a \delta r_{a;\boldsymbol{k}'\boldsymbol{k}} \tag{S28}$$

$$g_1^{(1)}(\boldsymbol{k},\omega) = \tau_{1\omega}'^{(1)}\left[\int_{\boldsymbol{k}'} w_{\boldsymbol{k}\boldsymbol{k}'}^{(A)}\tau_{1\omega}'^{(0)}\int_{\boldsymbol{k}''} w_{\boldsymbol{k}'\boldsymbol{k}''}^{(S)} f_0'(\boldsymbol{k}'')eE_a\delta r_{a;\boldsymbol{k}''\boldsymbol{k}'} + \int_{\boldsymbol{k}'} w_{\boldsymbol{k}\boldsymbol{k}'}^{(A)} f_0'(\boldsymbol{k}')eE_a\delta r_{a;\boldsymbol{k}'\boldsymbol{k}}\right] \tag{S29}$$

$$\begin{aligned}
&g_2^{(0)}(\boldsymbol{k},0)\\
&= \tau_2'^{(0)}\Bigg[eE_a^*\partial_{k_a} g_1^{(0)}(\boldsymbol{k},\omega) + \int_{\boldsymbol{k}'} w_{\boldsymbol{k}\boldsymbol{k}'}^{(S)}[f_1'^{(0)}(\boldsymbol{k}',\omega) + g_1'^{(0)}(\boldsymbol{k}',\omega)]eE_a^*\delta r_{a;\boldsymbol{k}'\boldsymbol{k}}\\
&\quad + \frac{1}{2}\int_{\boldsymbol{k}'} w_{\boldsymbol{k}\boldsymbol{k}'}^{(S)} f_0''(\boldsymbol{k}')eE_a^*\delta r_{a;\boldsymbol{k}'\boldsymbol{k}}eE_b\delta r_{b;\boldsymbol{k}'\boldsymbol{k}}\Bigg] + \text{c.c.}\\
&= \tau_2'^{(0)}\Bigg[eE_a^*\partial_{k_a}\tau_{1\omega}'^{(0)}\int_{\boldsymbol{k}'} w_{\boldsymbol{k}\boldsymbol{k}'}^{(S)} f_0'(\boldsymbol{k}')eE_b\delta r_{b;\boldsymbol{k}'\boldsymbol{k}} + \int_{\boldsymbol{k}'} w_{\boldsymbol{k}\boldsymbol{k}'}^{(S)} eE_a^*\delta r_{a;\boldsymbol{k}'\boldsymbol{k}}\partial_{\epsilon_{\boldsymbol{k}'}}\tau_{1\omega}^{(0)}eE_b\partial_{k_b'} f_0(\boldsymbol{k}')\\
&\quad + \int_{\boldsymbol{k}'} w_{\boldsymbol{k}\boldsymbol{k}'}^{(S)} eE_a^*\delta r_{a;\boldsymbol{k}'\boldsymbol{k}}\partial_{\epsilon_{\boldsymbol{k}'}}\tau_{1\omega}'^{(0)}\int_{\boldsymbol{k}''} w_{\boldsymbol{k}'\boldsymbol{k}''}^{(S)} f_0'(\boldsymbol{k}'')eE_b\delta r_{b;\boldsymbol{k}''\boldsymbol{k}'}\\
&\quad + \frac{1}{2}\int_{\boldsymbol{k}'} w_{\boldsymbol{k}\boldsymbol{k}'}^{(S)} f_0''(\boldsymbol{k}')eE_a^*\delta r_{a;\boldsymbol{k}'\boldsymbol{k}}eE_b\delta r_{b;\boldsymbol{k}'\boldsymbol{k}}\Bigg] + \text{c.c.}
\end{aligned} \tag{S30}$$

$$
\begin{aligned}
& g_2^{(1)}(\boldsymbol{k},0) \\
&= \tau_2'^{(1)}\Bigg[eE_a^*\partial_{k_a} g_1^{(1)}(\boldsymbol{k},\omega) + \int_{\boldsymbol{k}'} w^{(S)}_{\boldsymbol{k}\boldsymbol{k}'}[f_1'^{(1)}(\boldsymbol{k}',\omega) + g_1'^{(1)}(\boldsymbol{k}',\omega)] eE_a^*\delta r_{a;\boldsymbol{k}'\boldsymbol{k}} + \int_{\boldsymbol{k}'} w^{(A)}_{\boldsymbol{k}\boldsymbol{k}'} g_2^{(0)}(\boldsymbol{k}',0) \\
&\quad + \int_{\boldsymbol{k}'} w^{(A)}_{\boldsymbol{k}\boldsymbol{k}'}[f_1'^{(0)}(\boldsymbol{k}',\omega) + g_1'^{(0)}(\boldsymbol{k}',\omega)] eE_a^*\delta r_{a;\boldsymbol{k}'\boldsymbol{k}} + \frac{1}{2}\int_{\boldsymbol{k}'} w^{(A)}_{\boldsymbol{k}\boldsymbol{k}'} f_0''(\boldsymbol{k}') eE_a^*\delta r_{a;\boldsymbol{k}'\boldsymbol{k}} eE_b\delta r_{b;\boldsymbol{k}'\boldsymbol{k}} \Bigg] \\
&\quad + \text{c.c.} \\
&= \tau_2'^{(1)}\Bigg\{ eE_a^*\partial_{k_a}\tau_{1\omega}'^{(1)} \left[\int_{\boldsymbol{k}'} w^{(A)}_{\boldsymbol{k}\boldsymbol{k}'}\tau_{1\omega}'^{(0)} \int_{\boldsymbol{k}''} w^{(S)}_{\boldsymbol{k}'\boldsymbol{k}''} f_0'(\boldsymbol{k}'') eE_b\delta r_{b;\boldsymbol{k}''\boldsymbol{k}'} + \int_{\boldsymbol{k}'} w^{(A)}_{\boldsymbol{k}\boldsymbol{k}'} f_0'(\boldsymbol{k}') eE_b\delta r_{b;\boldsymbol{k}'\boldsymbol{k}} \right] \\
&\quad + \int_{\boldsymbol{k}'} w^{(S)}_{\boldsymbol{k}\boldsymbol{k}'} eE_a^*\delta r_{a;\boldsymbol{k}'\boldsymbol{k}} \partial_{\epsilon_{\boldsymbol{k}'}} \Bigg[\tau_{1\omega}^{(1)} \int_{\boldsymbol{k}''} w^{(A)}_{\boldsymbol{k}'\boldsymbol{k}''}\tau_{1\omega}^{(0)} eE_b\partial_{k_b''} f_0(\boldsymbol{k}'') \\
&\qquad + \tau_{1\omega}'^{(1)} \int_{\boldsymbol{k}''} w^{(A)}_{\boldsymbol{k}'\boldsymbol{k}''}\tau_{1\omega}'^{(0)} \int_{\boldsymbol{k}'''} w^{(S)}_{\boldsymbol{k}''\boldsymbol{k}'''} f_0'(\boldsymbol{k}''') eE_b\delta r_{b;\boldsymbol{k}'''\boldsymbol{k}''} + \tau_{1\omega}'^{(1)} \int_{\boldsymbol{k}''} w^{(A)}_{\boldsymbol{k}'\boldsymbol{k}''} f_0'(\boldsymbol{k}'') eE_b\delta r_{b;\boldsymbol{k}''\boldsymbol{k}'} \Bigg] \\
&\quad + \int_{\boldsymbol{k}'} w^{(A)}_{\boldsymbol{k}\boldsymbol{k}'}\tau_2'^{(0)} \Bigg[eE_a^*\partial_{k_a'}\tau_{1\omega}'^{(0)} \int_{\boldsymbol{k}''} w^{(S)}_{\boldsymbol{k}'\boldsymbol{k}''} f_0'(\boldsymbol{k}'') eE_b\delta r_{b;\boldsymbol{k}''\boldsymbol{k}'} \\
&\qquad + \int_{\boldsymbol{k}''} w^{(S)}_{\boldsymbol{k}'\boldsymbol{k}''} eE_a^*\delta r_{a;\boldsymbol{k}''\boldsymbol{k}'}\partial_{\epsilon_{\boldsymbol{k}''}}\tau_{1\omega}^{(0)} eE_b\partial_{k_b''} f_0(\boldsymbol{k}'') \\
&\qquad + \int_{\boldsymbol{k}''} w^{(S)}_{\boldsymbol{k}'\boldsymbol{k}''} eE_a^*\delta r_{a;\boldsymbol{k}''\boldsymbol{k}'}\partial_{\epsilon_{\boldsymbol{k}''}}\tau_{1\omega}'^{(0)} \int_{\boldsymbol{k}'''} w^{(S)}_{\boldsymbol{k}''\boldsymbol{k}'''} f_0'(\boldsymbol{k}''') eE_b\delta r_{b;\boldsymbol{k}'''\boldsymbol{k}''} \\
&\qquad + \frac{1}{2}\int_{\boldsymbol{k}''} w^{(S)}_{\boldsymbol{k}'\boldsymbol{k}''} f_0''(\boldsymbol{k}'') eE_a^*\delta r_{a;\boldsymbol{k}''\boldsymbol{k}'} eE_b\delta r_{b;\boldsymbol{k}''\boldsymbol{k}'} \Bigg] \\
&\quad + \int_{\boldsymbol{k}'} w^{(A)}_{\boldsymbol{k}\boldsymbol{k}'} eE_a^*\delta r_{a;\boldsymbol{k}'\boldsymbol{k}} \left[\tau_{1\omega}^{(0)} eE_b\partial_{k_a} f_0'(\boldsymbol{k}) + \partial_{\epsilon_{\boldsymbol{k}'}}\tau_{1\omega}'^{(0)} \int_{\boldsymbol{k}''} w^{(S)}_{\boldsymbol{k}'\boldsymbol{k}''} f_0'(\boldsymbol{k}'') eE_b\delta r_{b;\boldsymbol{k}''\boldsymbol{k}'} \right] \\
&\quad + \frac{1}{2}\int_{\boldsymbol{k}'} w^{(A)}_{\boldsymbol{k}\boldsymbol{k}'} f_0''(\boldsymbol{k}') eE_a^*\delta r_{b;\boldsymbol{k}'\boldsymbol{k}} eE_b\delta r_{b;\boldsymbol{k}'\boldsymbol{k}} \Bigg\} + \text{c.c.}
\end{aligned}
\tag{S31}
$$

$\tau_{n\omega}^{(m)}$ and $\tau_{n\omega}'^{(m)}$ are the shorthand notations for

$$
\tau_{n\omega}^{(m)} = \frac{\tau_n^{(m)}}{1 - i\omega\tau_n^{(m)}}, \quad \tau_{n\omega}'^{(m)} = \frac{\tau_n'^{(m)}}{1 - i\omega\tau_n'^{(m)}} \tag{S32}
$$

Those formal solutions find the scattering time dependence of the distribution functions for low frequencies ($\omega\tau \ll 1$)

$$
\begin{aligned}
f_n^{\text{scatt}} &\propto \tau^n E^n, \\
f_n^{\text{adist}} &\propto (\tau^0 E^n, \tau^1 E^n, \ldots, \tau^{n-1} E^n)
\end{aligned}
\tag{S33}
$$

Higher-order corrections for the anomalous distribution ($n \geq 2$) has a nested structure of f_{n-1}^{scatt} and f_{n-1}^{adist}. In the weak disorder limit of $\tau \to \infty$, we obtain

$$f_n^{\mathrm{adist}} \propto \tau^{n-1} E^n \tag{S34}$$

We can define another scattering time $\tilde{\tau}$ from the antisymmetric part $w^{(A)}$. It is roughly speaking given by

$$\int_{\boldsymbol{k}'} w^{(A)}_{\boldsymbol{k}\boldsymbol{k}'} f(\boldsymbol{k}') \sim \frac{1}{\tilde{\tau}} f(\boldsymbol{k}) \tag{S35}$$

We note that the definition of $\tilde{\tau}$ is accompanied with the distribution function because the optical theorem for elastic scattering concludes Eq. S8.

Section S2. Current response

From the distribution function, the electric current response is obtained by

$$\boldsymbol{j} = -e \int_{\boldsymbol{k}} \boldsymbol{v}(\boldsymbol{k}) f(\boldsymbol{k}) \tag{S36}$$

$\boldsymbol{v}(\boldsymbol{k})$ is the electron's group velocity, given by

$$\begin{aligned} \boldsymbol{v} &= \frac{\partial \epsilon_{\boldsymbol{k}}}{\partial \boldsymbol{k}} - \dot{\boldsymbol{k}} \times \boldsymbol{\Omega} + \int_{\boldsymbol{k}'} w_{\boldsymbol{k}'\boldsymbol{k}} \delta \boldsymbol{r}_{\boldsymbol{k}'\boldsymbol{k}} \\ &\equiv \boldsymbol{v}_0 + \boldsymbol{v}_{\mathrm{av}} + \boldsymbol{v}_{\mathrm{sj}} \end{aligned} \tag{S37}$$

The group velocity from the energy band dispersion $\boldsymbol{v}_0$ is independent of the Berry curvature, while the Berry curvature induces the anomalous velocity $\boldsymbol{v}_{\mathrm{av}}$ (*57–59*) and the side-jump velocity $\boldsymbol{v}_{\mathrm{sj}}$ (*60*)

$$\boldsymbol{v}_{\mathrm{av}} = -\dot{\boldsymbol{k}} \times \boldsymbol{\Omega} = e\boldsymbol{E} \times \boldsymbol{\Omega} \tag{S38}$$

$$\boldsymbol{v}_{\mathrm{sj}} = \int_{\boldsymbol{k}'} w_{\boldsymbol{k}'\boldsymbol{k}} \delta \boldsymbol{r}_{\boldsymbol{k}'\boldsymbol{k}} \tag{S39}$$

In terms of the electric field E, $\boldsymbol{v}_{\rm av}$ is linear in E whereas $\boldsymbol{v}_0$ and $\boldsymbol{v}_{\rm sj}$ do not depend on E. Lastly, only the side-jump velocity depends on the scattering time: $\boldsymbol{v}_{\rm sj} \propto \tau^{-1}$. Since there is no current in equilibrium, the electric current is described by (*29, 54*)

$$\boldsymbol{j} = -e \int_{\boldsymbol{k}} (\boldsymbol{v}_0 + \boldsymbol{v}_{\rm av} + \boldsymbol{v}_{\rm sj})(f^{\rm scatt} + f^{\rm adist}) \tag{S40}$$

which allows us to decompose the current into contributions of different origins. We note that the contribution from the anomalous distribution $f^{\rm adist}$ could be recognized as a part of the side-jump effect since it is originated both from the Berry curvature and scattering.

Before calculating the second-order conductivity, we note the problem about the energy dissipation or Joule heating because of $\boldsymbol{j} \cdot \boldsymbol{E} \neq 0$; see also e.g., Ref. (*28*) for discussions. This concludes that a stationary state solution cannot be obtained for a closed system with energy conservation. To circumvent this issue, we neglect parts of the distribution function which are isotropically coupled to the electric field. To be more explicit, the distribution function at the second order in the electric field involves a term proportional to $|\boldsymbol{E}|^2 f_0''$. Technically, such an excess term arises when we substitute a distribution function f_n ($n \geq 1$) into the collision integral $C[f]$, which involves only elastic scattering. Since this term is isotropic, it cannot be relaxed by elastic scattering, which conserves energy, so that a stationary state solution does not exist. Inelastic scattering resolves the problem as it does not conserve energy and excess energy is dissipated as heat. Note that an inelastic scattering time is typically much longer than an elastic scattering time. In calculating the second-order conductivity, we simply subtract and neglect such isotropic terms although they potentially change the temperature for a closed system. Importantly, they do not contribute to current from the band velocity since $\int_{\boldsymbol{k}} \boldsymbol{v}_0 f_0'' = \int_{\boldsymbol{k}} \nabla_{\boldsymbol{k}} f_0' = 0$.

We can see the six possible combinations in Eq. S40. For the second-order current re-

sponse, the scattering time dependence of each contribution for low frequencies $\omega\tau \ll 1$ is

$$\boldsymbol{v}_0 f_2^{\mathrm{scatt}} \propto \tau^2, \quad \boldsymbol{v}_{\mathrm{av}} f_1^{\mathrm{scatt}} \propto \tau^1, \quad \boldsymbol{v}_{\mathrm{sj}} f_2^{\mathrm{scatt}} \propto \tau^1 \tag{S41}$$

$$\boldsymbol{v}_0 f_2^{\mathrm{adist}} \propto (\tau^1, \tau^0), \quad \boldsymbol{v}_{\mathrm{av}} f_1^{\mathrm{adist}} \propto \tau^0, \quad \boldsymbol{v}_{\mathrm{sj}} f_2^{\mathrm{adist}} \propto (\tau^0, \tau^{-1}) \tag{S42}$$

In the weak disorder limit of $\tau \to \infty$, the first term, the skew scattering contribution, $\boldsymbol{v}_0 f^{\mathrm{scatt}}$ predominates, which we focus on in this work. This is equivalent to neglect all Berry curvature related effects. The second-order current response arising from this term is

$$\boldsymbol{j}_2 = -e \int_{\boldsymbol{k}} \boldsymbol{v}_0(\boldsymbol{k}) f_2^{\mathrm{scatt}}(\boldsymbol{k}) = -e \int_{\boldsymbol{k}} \boldsymbol{v}_0(\boldsymbol{k}) [f_2^{(0)}(\boldsymbol{k}) + f_2^{(1)}(\boldsymbol{k})] \tag{S43}$$

We define the second-order conductivity by the relation

$$j_{2,a} = \chi_{abc} E_b^* E_c \tag{S44}$$

and we obtain from Eqs. S26 and S27

$$\chi_{abc} = \chi_{abc}^{(0)} + \chi_{abc}^{(1)} \tag{S45}$$

$$\chi_{abc}^{(0)} = -e^3 \tau_2^{(0)} \tau_{1\omega}^{(0)} \int_{\boldsymbol{k}} v_{0,a} \partial_{k_b} \partial_{k_c} f_0(\boldsymbol{k}) + (b \leftrightarrow c)^* \tag{S46}$$

$$\begin{aligned} \chi_{abc}^{(1)} = -e^3 \Bigg[& \tau_2^{(1)} \tau_{1\omega}^{(1)} \tau_{1\omega}^{(0)} \int_{\boldsymbol{k}} v_{0,a} \partial_{k_b} \int_{\boldsymbol{k}'} w^{(A)}_{s,\boldsymbol{k}\boldsymbol{k}'} \partial_{k_c'} f_0(\boldsymbol{k}') \\ & + \tau_2^{(1)} \tau_2^{(0)} \tau_{1\omega}^{(0)} \int_{\boldsymbol{k}} v_{0,a} \int_{\boldsymbol{k}'} w^{(A)}_{s,\boldsymbol{k}\boldsymbol{k}'} \partial_{k_b'} \partial_{k_c'} f_0(\boldsymbol{k}') \Bigg] \\ & + (b \leftrightarrow c)^* \end{aligned} \tag{S47}$$

$\chi_{abc}^{(0)}$ vanishes identically in time-reversal-invariant systems because of $\epsilon_{\boldsymbol{k}} = \epsilon_{-\boldsymbol{k}}$; it follows from $\boldsymbol{v}_0(\boldsymbol{k}) = -\boldsymbol{v}_0(-\boldsymbol{k})$, and we see that the integrand is odd in $\boldsymbol{k}$ for $\chi_{abc}^{(0)}$. Therefore, the second-order contribution from the skew-scattering contribution arises from $\chi_{abc}^{(1)}$, i.e., $\chi_{abc} = \chi_{abc}^{(1)}$.

To calculate the second-order response, it is useful to express Eqs. S46 and S47 in the

following forms

$$\begin{aligned}\chi^{(0)}_{abc} &= -e^3\tau^{(0)}_2\tau^{(0)}_{1\omega}\int_{\boldsymbol{k}}[-f_0'(\boldsymbol{k})]v_{0,a}(\partial_{k_b}\partial_{k_c}\epsilon_{\boldsymbol{k}}) + (b\leftrightarrow c)^* \\ &= -2e^3\,\mathrm{Re}\left[\tau^{(0)}_2\tau^{(0)}_{1\omega}\right]\int_{\boldsymbol{k}}[-f_0'(\boldsymbol{k})]v_{0,a}(\partial_{k_b}\partial_{k_c}\epsilon_{\boldsymbol{k}})\end{aligned} \tag{S48}$$

$$\begin{aligned}\chi^{(1)}_{abc} = -e^3\Bigg[&\tau^{(1)}_2\tau^{(1)}_{1\omega}\tau^{(0)}_{1\omega}\int_{\boldsymbol{k}}[-f_0'(\boldsymbol{k})](\partial_{k_a}\partial_{k_b}\epsilon_{\boldsymbol{k}})\int_{\boldsymbol{k}'}w^{(A)}_{\boldsymbol{k}\boldsymbol{k}'}v_{0,c} \\ &- \tau^{(1)}_2\tau^{(0)}_2\tau^{(0)}_{1\omega}\int_{\boldsymbol{k}}[-f_0'(\boldsymbol{k})]v_{0,a}\int_{\boldsymbol{k}'}w^{(A)}_{\boldsymbol{k}\boldsymbol{k}'}(\partial_{k_b}\partial_{k_c}\epsilon_{\boldsymbol{k}}) \\ &+ \tau^{(1)}_2\tau^{(0)}_2\tau^{(0)}_{1\omega}\int_{\boldsymbol{k}}[-f_0'(\boldsymbol{k})]\partial_{k_a}\int_{\boldsymbol{k}'}w^{(A)}_{\boldsymbol{k}\boldsymbol{k}'}v_{0,b}v_{0,c}\Bigg] \\ &+ (b\leftrightarrow c)^*\end{aligned} \tag{S49}$$

We also show the expression for $\chi^{(0)}_{abc}$ for reference although it vanishes. These expressions show that results at finite temperature can be obtained by considering the thermal broadening of the Fermi–Dirac distribution, where the Fermi energy ϵ_F is replaced by the chemical potential μ_{chem} with the carrier density fixed. More explicitly, from the following relation

$$-f_0'(\boldsymbol{k}) = \int d\epsilon[-f_0'(\epsilon;\mu_{\mathrm{chem}})]\delta(\epsilon_{\boldsymbol{k}}-\epsilon_F) \tag{S50}$$

the second-order conductivity at finite temperature is obtained by

$$\chi_{abc}(\mu_{\mathrm{chem}},T) = \int d\epsilon[-f_0'(\epsilon;\mu_{\mathrm{chem}})]\chi_{abc}(\epsilon,T=0) \tag{S51}$$

2.1 Linear response

We also calculate the linear response to obtain responsivities (defined below). From the Boltzmann equation, the linear current response is given by

$$j_{1,a}(\omega) = \sigma_{ab}E_b(\omega) = -e\int_{\boldsymbol{k}}v_{0,a}f_1^{\mathrm{scatt}} \tag{S52}$$

leading to the linear conductivity

$$\sigma_{ab} = \sigma_{ab}^{(0)} + \sigma_{ab}^{(1)} \tag{S53}$$

$$\sigma_{ab}^{(0)} = -e^2\tau_{1\omega}^{(0)}\int_{\boldsymbol{k}} v_{0,a}\partial_{k_b} f_0(\boldsymbol{k}) = e^2\tau_{1\omega}^{(0)}\int_{\boldsymbol{k}} v_{0,a}v_{0,b}[-f_0'(\boldsymbol{k})] \tag{S54}$$

$$\sigma_{ab}^{(1)} = -e^2\tau_{1\omega}^{(1)}\tau_{1\omega}^{(0)}\int_{\boldsymbol{k}} v_{0,a}\int_{\boldsymbol{k}'} w_{\boldsymbol{k}\boldsymbol{k}'}^{(A)}\partial_{k_b'} f_0(\boldsymbol{k}') \tag{S55}$$

Section S3. Graphene-based models with trigonal lattice structures

Now we evaluate the current response for explicit models. We consider two graphene-based models, utilizing monolayer and bilayer graphene. The crystalline lattices belong to a crystallographic point group D_{3h} and C_{3v}, respectively. We note that inversion is equivalent to the in-plane two-fold rotation in 2D models, which is absent in the present models. Around K and K' points, $\boldsymbol{K} = \left(\frac{4\pi}{3\sqrt{3}}, 0\right)$ and $\boldsymbol{K}' = \left(-\frac{4\pi}{3\sqrt{3}}, 0\right)$, the $k\cdot p$ Hamiltonian to second order is

$$\begin{aligned} H_s(\boldsymbol{k}) &= \begin{pmatrix} \Delta & svk_{-s} - \lambda k_s^2 \\ svk_s - \lambda k_{-s}^2 & -\Delta \end{pmatrix} \\ &= \left[svk_x - \lambda(k_x^2 - k_y^2)\right]\sigma_x + \left(vk_y + 2s\lambda k_x k_y\right)\sigma_y + \Delta\sigma_z \end{aligned} \tag{S56}$$

where k_x and k_y are measured from K or K' point, labeled by $s = \pm 1$, and k_s is defined by $k_s = k_x + isk_y$. The energy dispersion of the positive branch is given by

$$\epsilon_{\boldsymbol{k}} = \sqrt{v^2k^2 + \lambda^2k^4 + \Delta^2 - 2sv\lambda k^3\cos 3\theta} \tag{S57}$$

and the corresponding normalized wavefunction is

$$|\boldsymbol{k}, s\rangle = \frac{1}{\sqrt{2\,\epsilon_{\boldsymbol{k}}(\epsilon_{\boldsymbol{k}} + \Delta)}}\begin{pmatrix} \epsilon_{\boldsymbol{k}} + \Delta \\ \left[svk_x - \lambda(k_x^2 - k_y^2)\right] + i\left(vk_y + 2s\lambda k_x k_y\right) \end{pmatrix} \tag{S58}$$

The Berry curvature is also calculated as

$$\Omega_z = -\frac{s\Delta(v^2 - 4\lambda^2k^4)}{2\epsilon_{\boldsymbol{k}}^3} \tag{S59}$$

The Hamiltonian Eq. S56 is available to both monolayer and bilayer models (Fig. S1). The Pauli matrix σ_a describes the two sublattices for monolayer graphene and two layers for AB (Bernal) stacked bilayer graphene. Another difference is found in which of v and λ is dominant, which is explained later. Δ describes the potential energy difference at the two sublattice sites or layers, which opens a gap to the energy spectrum. In the following, we consider the two cases separately.

3.1 Monolayer graphene

For monolayer graphene, the terms with v dominate those with λ ($vk_F \gg \lambda k_F^2$), where λ characterizes the trigonal warping of the Fermi surface. $s = +1$ corresponds to K valley and $s = -1$ to K' valley. The Dirac mass can be induced for example by placing a graphene sheet on a hexagonal boron nitride (hBN) substrate. For a tight-binding model on a honeycomb lattice with the nearest-neighbor hopping amplitude t and the distance between sites a, the velocity v and the trigonal warping λ are given by $v = 3ta/2$ and $\lambda = 3ta^2/8$, respectively (*40, 41*).

We assume that the trigonal warping is small and obtain the energy dispersion $\epsilon_{\boldsymbol{k}}$ to first order in λ as

$$\epsilon_{\boldsymbol{k}} = \sqrt{v^2k^2 + \Delta^2} - sv\lambda \frac{k^3}{\sqrt{v^2k^2 + \Delta^2}} \cos 3\theta_{\boldsymbol{k}} + O(\lambda^2) \tag{S60}$$

where the Fermi wavevector k_F is given by

$$k_F = \frac{\sqrt{\epsilon_F^2 - \Delta^2}}{v} \tag{S61}$$

The density of states (DOS) at the Fermi energy is

$$D_0 = \frac{\epsilon_F}{2\pi v^2} \tag{S62}$$

and $\theta_{\boldsymbol{k}}$ denotes the polar angle of $\boldsymbol{k}$. The Fermi surface can be parameterized by $\theta_{\boldsymbol{k}}$ as

$$k(\theta_{\boldsymbol{k}}) = k_F + s\lambda \frac{k_F^2}{v} \cos 3\theta_{\boldsymbol{k}} \tag{S63}$$

To evaluate the scattering rate, we need the wavefunction on the Fermi surface. The normalized wavefunction on the Fermi surface is given by

$$|\boldsymbol{k}, s\rangle = \left(\sqrt{\frac{\epsilon_F + \Delta}{2\epsilon_F}}, \frac{(s\cos\theta_{\boldsymbol{k}} + i\sin\theta_{\boldsymbol{k}})(vk_F + i\lambda k_F^2 \sin 3\theta_{\boldsymbol{k}})}{\sqrt{2\epsilon_F(\epsilon_F + \Delta)}} \right)^T \tag{S64}$$

Also, it is useful to see the Berry curvature on the Fermi surface, which is given by

$$\Omega_z = -\frac{sv^2\Delta}{2\epsilon_F^3} + O(\lambda^2) \tag{S65}$$

The second-order conductivity is considered in the presence of an elastic impurity scattering. Here, we assume short-ranged random scalar impurities

$$V(\boldsymbol{r}) = V_i \sum_j \delta(\boldsymbol{r} - \boldsymbol{r}_j) \tag{S66}$$

but restrict scattering within each valley. V_i is the impurity potential strength, n_i is the impurity density, and $\boldsymbol{r}_j$ denotes an impurity position, where the summation is taken over all impurity sites. Then, we obtain the scattering rates for the valley s to first order in λ as

$$\begin{aligned} w^{(S)}_{s,\boldsymbol{k}\boldsymbol{k}'} = \frac{\pi n_i V_i^2}{2\epsilon_F^2(\epsilon_F + \Delta)^2} \Big[&|(\epsilon_F + \Delta)^2 + v^2 k_F^2 e^{i(\theta - \theta')}|^2 \\ &- 2s\lambda v k_F^3 (\epsilon_F + \Delta)^2 \sin(\theta - \theta')(\sin 3\theta - \sin 3\theta') \Big] \delta(\epsilon_{\boldsymbol{k}} - \epsilon_{\boldsymbol{k}'}) \end{aligned} \tag{S67}$$

$$\begin{aligned} w^{(A)}_{s,\boldsymbol{k}\boldsymbol{k}'} = -\frac{\pi n_i V_i^3 \Delta k_F^2}{2\epsilon_F^2} \Big\{ &s\sin(\theta - \theta') \\ &+ \lambda \frac{k_F}{v} [\sin(\theta - 4\theta') + \sin(4\theta - \theta') - \sin(\theta + 2\theta') + \sin(2\theta + \theta')] \Big\} \delta(\epsilon_{\boldsymbol{k}} - \epsilon_{\boldsymbol{k}'}) \end{aligned} \tag{S68}$$

with $\theta = \theta_{\boldsymbol{k}}$ and $\theta' = \theta_{\boldsymbol{k}'}$ parametrizing the Fermi surface.

In order to obtain the distribution function, we need to determine the scattering times that satisfy the relation Eq. S22. For the present Hamiltonian, the scattering times are obtained as

$$\tau_1^{(0)} = \tau_1^{(1)} = \tau_2^{(1)} = \left(n_i V_i^2 \frac{\epsilon_F^2 + 3\Delta^2}{4v^2\epsilon_F} \right)^{-1} \tag{S69}$$

$$\tau_1^{(1)} = \left(n_i V_i^2 \frac{\epsilon_F^2 + \Delta^2}{2v^2\epsilon_F} \right)^{-1} \tag{S70}$$

These solutions are obtained to $O(\lambda^0)$, which are enough to evaluate conductivities to order $O(\lambda^1)$ (see the next paragraph). Also, there is no directional dependence in the scattering times at order λ^0. For clarity, we define

$$\tau = \left(n_i V_i^2 \frac{\epsilon_F^2 + 3\Delta^2}{4v^2 \epsilon_F} \right)^{-1} \tag{S71}$$

and the dimensionless quantity

$$\gamma = \frac{\epsilon_F^2 + 3\Delta^2}{2(\epsilon_F^2 + \Delta^2)} (\leq 1) \tag{S72}$$

which are defined to satisfy $\tau_1^{(0)} = \tau_1^{(1)} = \tau_2^{(1)} = \tau$ and $\tau_1^{(1)} = \gamma\tau$

We calculate the second-order contribution from each valley separately, namely $\chi_{abc} = \chi_{abc}^{(0)} + \chi_{abc}^{(1)}$ with

$$\chi_{abc}^{(0)} = \sum_s \chi_{s,abc}^{(0)}, \quad \chi_{abc}^{(1)} = \sum_s \chi_{s,abc}^{(1)} \tag{S73}$$

The contributions from each valley s are obtained from Eqs. S46 and S47 at zero temperature as

$$\chi_{s,xxx}^{(0)} = -\chi_{s,xyy}^{(0)} = -\chi_{s,yxy}^{(0)} = -\chi_{s,yyx}^{(0)} = se^3\tau^2 v \frac{3\lambda k_F^2(\epsilon_F^2 + \Delta^2)\gamma}{\pi\epsilon_F^3} \operatorname{Re}\left[\frac{1}{1 - i\omega\tau} \right] \tag{S74}$$

$$\chi_{s,xxy}^{(1)} = \chi_{s,xyx}^{(1)} = \chi_{s,yxx}^{(1)} = -\chi_{s,yyy}^{(1)} = 4e^3\tau^2 v \frac{\tau}{\tilde{\tau}} \operatorname{Re}\left[\frac{v k_F(2\epsilon_F^2 + \Delta^2)}{(1 - i\omega\tau)^2 \pi\epsilon_F^3} - \gamma \frac{v k_F(\epsilon_F^2 + 2\Delta^2)}{(1 - i\omega\tau)\pi\epsilon_F^3} \right] \tag{S75}$$

where the factor of two from spin is multiplied. We note that D_{3h} symmetry concludes that the imaginary part of the second-order DC conductivity vanishes (*29*) and that the system does not have second-order response to a circularly-polarized field. We define another scattering time $\tilde{\tau}$, related to $w^{(A)}$ (see Eq. S35), as

$$\tilde{\tau} = \left(\Delta\lambda \frac{n_i V_i^3 k_F^3}{8v^3 \epsilon_F} \right)^{-1} \tag{S76}$$

This quantity measures the amounts of inversion breaking (m) and the Fermi surface warping (λ). The ratio $\tau/\tilde{\tau}$ becomes

$$\frac{\tau}{\tilde{\tau}} = \Delta\lambda \frac{V_i k_F^3}{2v(\epsilon_F^2 + 3\Delta^2)} = \frac{1}{2} \frac{\Delta \cdot V_i k_F^2}{\epsilon_F^2 + 3\Delta^2} \frac{\lambda k_F^2}{v k_F} \tag{S77}$$

Roughly speaking, the ratio is determined by the product of the following dimensionless quantities: inversion breaking Δ/ϵ_F, the Fermi surface warping $\lambda k_F^2/(vk_F)$, and the impurity strength $V_i k_F^2/\epsilon_F$. We can see from Eq. S68 that the antisymmetric scattering becomes finite when inversion is broken by $\Delta \neq 0$ but it does not require finite Fermi surface warping λ. However, the second-order response vanishes when the Fermi surface warping is absent. The ratio $\tau/\tilde{\tau}$ measures the amount of the contribution to the second-order response from skew scattering, but not the magnitude of skew scattering itself.

$\chi^{(0)}$ is originated from the absence of time-reversal or inversion symmetry within each valley, resulting from the Fermi surface anisotropy. However, time reversal is preserved with the two valleys, and thus contributions from different valleys cancel. This effect of $\chi^{(0)}$ can be seen in Fig. 2C, where the two valleys generates the opposite static velocity $\boldsymbol{V}$. In contrast, $\chi^{(1)}$ adds up with the two valleys, since this contribution captures the opposite chirality of the wavefunctions around each valley, which is not visible from the Fermi surface shape. Finally, we obtain the nonvanishing elements of the second-order conductivity

$$\chi_{xxy} = \chi_{xyx} = \chi_{yxx} = -\chi_{yyy} = -4e^3 v_F \frac{\tau^3}{\tilde{\tau}} \zeta(\omega) \equiv -\chi(\omega) \tag{S78}$$

with the average Fermi velocity on the Fermi surface

$$v_F = \frac{v^2 k_F}{\epsilon_F} \tag{S79}$$

and the dimensionless function

$$\zeta(\omega) = \frac{2}{\pi} \mathrm{Re} \left[\gamma \frac{\epsilon_F^2 + 2\Delta^2}{(1 - i\omega\tau)\epsilon_F^2} - \frac{2\epsilon_F^2 + \Delta^2}{(1 - i\omega\tau)^2 \epsilon_F^2} \right] \tag{S80}$$

Here the factor of four in Eq. S78 corresponds to spin and valley degrees of freedom. The finite elements of χ_{abc} are consistent with D_{3h} symmetry of the lattice.

3.1.1 Linear conductivity and responsivity

To estimate the magnitude of the second-order response and to calculate responsivities, we also calculate the linear conductivity, particularly $\sigma^{(0)}_{s,ab}$. From Eq. S54, we obtain

$$\sigma^{(0)}_{s,ab} = 2e^2\tau^{(0)}_{1\omega}\frac{v^2k_F^2}{4\pi\epsilon_F}\delta_{ab} \tag{S81}$$

for each valley with the spin degrees of freedom included. The linear conductivity is diagonal, and hence we write

$$\sigma(\omega) = \sum_s \mathrm{Re}\,\sigma^{(0)}_{s,aa} = e^2\tau\frac{v^2k_F^2}{\pi\epsilon_F}\frac{1}{1+(\omega\tau)^2} \tag{S82}$$

Since the linear conductivity can be written as $\sigma = ne\mu$ with the electron density n and the mobility μ, in low frequencies we find the relation

$$\mu = e\tau\frac{v^2}{\epsilon_F} \tag{S83}$$

We note that the electron density is obtained by $n = k_F^2/\pi$.

The short-circuit current responsivity $\Re_I$ is defined as the ratio of the generated DC current j_2 to the power of the incident electric field absorbed by the sample. When a sample has a dimension of L^2 and the incident field is uniform on the sample, the current responsivity is given by

$$\Re_I \equiv \frac{j_2L}{j_1EL^2} = \frac{1}{L}\frac{\chi(\omega)}{\sigma(\omega)} \tag{S84}$$

We note that the dimension L corresponds to either width or length of a sample, depending on whether the second-order response of interest is longitudinal or transverse to the incident electric field. We also define the voltage responsivity $\Re_V$ as the ratio of the voltage generated by the second-order response to the incident power:

$$\Re_V = \frac{j_2L/\sigma(0)}{j_1EL^2} = \frac{1}{L}\frac{\chi(\omega)}{\sigma(\omega)\sigma(0)} \tag{S85}$$

Both current responsivity $\Re_I$ and voltage responsivity $\Re_V$ depend on the sample dimension L and the ratio $\tau/\tilde{\tau}$. To remove those factors, we define the reduced current responsivity η_I and the reduced voltage responsivity η_V as follows

$$\Re_V = \eta_I \frac{1}{L}\frac{\tau}{\tilde{\tau}} \tag{S86}$$

$$\Re_I = \eta_V \frac{1}{L}\frac{\tau}{\tilde{\tau}} \tag{S87}$$

For the present model, η_I and η_V are obtained as

$$\eta_I = \frac{4\pi e\tau}{k_F}[1 + (\omega\tau)^2]\zeta(\omega) \tag{S88}$$

$$\eta_V = \frac{4\pi}{env_F}\left[1 + (\omega\tau)^2\right]\zeta(\omega) \tag{S89}$$

3.2 Bilayer graphene

Bernal stacked bilayer graphene has C_{3v} symmetry when the two layer have different potential energies. Because of the symmetry, we can use the same Hamiltonian Eq. S56; however, v is treated as a perturbation instead of λ for the bilayer case ($\lambda k_F^2 \gg v k_F$), as we can see from a tight-binging Hamiltonian (*40, 41*). Treating v as a perturbation, we obtain the energy dispersion $\epsilon_{\boldsymbol{k}}$ to first order in v as

$$\epsilon_{\boldsymbol{k}} = \sqrt{\lambda^2 k^4 + \Delta^2} - \frac{2sv\lambda k^3}{\sqrt{\lambda^2 k^4 + \Delta^2 \cos 3\theta_{\boldsymbol{k}}}} \tag{S90}$$

The DOS at the Fermi energy D_0 is given by

$$D_0 = \frac{\epsilon_F \Delta^2}{\pi k_F^2} \tag{S91}$$

The normalized wavefunction on the Fermi surface to order v is

$$|\boldsymbol{k}, s\rangle = \left(\sqrt{\frac{\epsilon_F + \Delta}{2\epsilon_F}}, -\frac{(\cos 2\theta_{\boldsymbol{k}} - is \sin 2\theta_{\boldsymbol{k}})(\lambda k_F^2 - ivk_F \sin 3\theta_{\boldsymbol{k}})}{\sqrt{2\epsilon_F(\epsilon_F + \Delta)}}\right)^T \tag{S92}$$

where k_F is defined by

$$k_F = \left(\frac{\epsilon_F^2 - \Delta^2}{\lambda^2} \right)^{1/4} \tag{S93}$$

The Berry curvature on the Fermi surface is

$$\Omega_z = \frac{2s\Delta\lambda^2 k_F^2}{\epsilon_F^3} + \frac{2\Delta v\lambda k_F \cos 3\theta}{\epsilon_F^3} + O(v^2) \tag{S94}$$

Using the wavefunction, we obtain the symmetric and antisymmetric scattering rates $w^{(S)}$ and $w^{(A)}$, respectively

$$w^{(S)}_{s,\boldsymbol{k}\boldsymbol{k}'} = \frac{\pi n_i V_i^2}{2\epsilon_F^2(\epsilon_F + \Delta)^2} \Big[\Big| (\epsilon_F + \Delta)^2 + \lambda^2 k_F^4 e^{2i(\theta-\theta')} \Big|^2 - 2sv\lambda(\epsilon_F + \Delta)^2 k_F^3 \sin(2\theta - 2\theta')(\sin 3\theta - \sin 3\theta') \Big] \delta(\epsilon_{\boldsymbol{k}} - \epsilon_{\boldsymbol{k}'}) \tag{S95}$$

$$w^{(A)}_{s,\boldsymbol{k}\boldsymbol{k}'} = \frac{\pi n V_i^3 k_F^2 \Delta}{4\epsilon_F^2} \Big\{ s \sin(2\theta - 2\theta') + \frac{v}{2\lambda k_F} \left[\sin(\theta + 2\theta') - \sin(2\theta + \theta') + \sin(2\theta - 5\theta') + \sin(5\theta - 2\theta') \right] \Big\} \delta(\epsilon_{\boldsymbol{k}} - \epsilon_{\boldsymbol{k}'}) \tag{S96}$$

For the bilayer case, the scattering times become

$$\tau_1^{(0)} = \left(\frac{n_i V_i^2 (\epsilon_F^2 + \Delta^2)}{4\lambda^2 k_F^2 \epsilon_F} \right)^{-1} \tag{S97}$$

$$\tau_1^{(1)} = \tau_2^{(0)} = \tau_2^{(1)} = \left(\frac{n_i V_i^2 (\epsilon_F^2 + 3\Delta^2)}{8\lambda^2 k_F^2 \epsilon_F} \right)^{-1} \tag{S98}$$

$$\tilde{\tau} = \left(\Delta v \frac{n_i V_i^3}{32\lambda^3 k_F \epsilon_F} \right)^{-1} \tag{S99}$$

We define τ as

$$\tau = \left(\frac{n_i V_i^2 (\epsilon_F^2 + \Delta^2)}{4\lambda^2 k_F^2 \epsilon_F} \right)^{-1} \tag{S100}$$

resulting in $\tau_1^{(0)} = \tau$ and $\tau_1^{(1)} = \tau_2^{(0)} = \tau_2^{(1)} = \gamma^{-1}\tau$, with the same γ for the monolayer case.

The contributions to the second-order conductivity from valley s are obtained from Eqs. S46 and S47 at zero temperature as

$$\chi^{(0)}_{s,xxx} = -\chi^{(0)}_{s,xyy} = -\chi^{(0)}_{s,yxy} = -\chi^{(0)}_{s,yyx} = se^3\tau^2 \frac{2\lambda k_F^2(\epsilon_F^2 + 2\Delta^2)}{\pi\epsilon_F^3\gamma} \,\mathrm{Re}\left[\frac{1}{1 - i\omega\tau}\right] \tag{S101}$$

$$\begin{aligned} \chi^{(1)}_{s,xxy} &= \chi^{(1)}_{s,xyx} = \chi^{(1)}_{s,yxx} = -\chi^{(1)}_{s,yyy} \\ &= e^3\tau^2(2\lambda k_F)\frac{\tau}{\tilde{\tau}}\frac{\lambda k_F^2\Delta^2}{4\pi\epsilon_F^3\gamma^2} \,\mathrm{Re}\left[\frac{5}{(1 - i\omega\tau)(1 - i\omega\gamma^{-1}\tau)} - \frac{6}{1 - i\omega\tau}\right] \end{aligned} \tag{S102}$$

For the bilayer model, the ratio $\tau/\tilde{\tau}$ is given by

$$\frac{\tau}{\tilde{\tau}} = \Delta v \frac{k_F V_i}{8\lambda(\epsilon_F^2 + \Delta^2)} \tag{S103}$$

Similarly to the monolayer case, $\chi^{(0)}_{s,abc}$ from each valley cancels but $\chi^{(1)}_{s,abc}$ adds up, leading to the second-order conductivity

$$\chi_{xxy} = \chi_{xyx} = \chi_{yxx} = -\chi_{yyy} = -4e^3 v_F \frac{\tau^3}{\tilde{\tau}}\zeta(\omega) \equiv -\chi(\omega) \tag{S104}$$

where for the bilayer model the average velocity on the Fermi surface v_F is

$$v_F = \frac{2\lambda^2 k_F^3}{\epsilon_F} \tag{S105}$$

and the dimensionless function $\zeta(\omega)$ becomes

$$\zeta(\omega) = \frac{\Delta^2}{8\pi\epsilon_F^2\gamma^2} \,\mathrm{Re}\left[\frac{6}{1 - i\omega\tau} - \frac{5}{(1 - i\omega\tau)(1 - i\omega\gamma^{-1}\tau)}\right] \tag{S106}$$

3.2.1 Linear conductivity and responsivity

We also evaluate the linear conductivity $\sigma^{(0)}_{s,ab}$ for each valley s with the spin degrees of freedom included (Eq. S54)

$$\sigma^{(0)}_{s,ab} = e^2\tau^{(0)}_{1\omega}\frac{\lambda^2 k_F^4}{\pi\epsilon_F}\delta_{ab} \tag{S107}$$

Similarly to the monolayer case, we define

$$\sigma(\omega) = \sum_s \mathrm{Re}\,\sigma^{(0)}_{s,aa} = e^2\tau\frac{\lambda^2 k_F^4}{\pi\epsilon_F}\frac{1}{1 + (\omega\tau)^2} \tag{S108}$$

For low frequencies, the mobility is calculated from the relation $\sigma = ne\mu$ by

$$\mu = e\tau \frac{2\lambda^2 k_F^2}{\epsilon_F} \tag{S109}$$

where the electron density is $n = k_F^2/\pi$.

For the bilayer case, the reduced current responsivity becomes

$$\eta_I = \frac{\chi(\omega)}{\sigma(\omega)} = \frac{8\pi e\tau}{k_F}[1 + (\omega\tau)^2]\zeta(\omega) \tag{S110}$$

and the reduced voltage responsivity is

$$\eta_V = \frac{\chi(\omega)}{\sigma(\omega)\sigma(0)} = \frac{16\pi}{env_F}\left[1 + (\omega\tau)^2\right]\zeta(\omega) \tag{S111}$$

Section S4. Estimate of parameters

Parameters for a realistic evaluation are taken and estimated from experiments on monolayer and bilayer graphene. For monolayer graphene on an hBN substrate, the imbalance of the potential energy within a sublattice is induced by the substrate and the lattice mismatch of graphene and hBN creates a superlattice with a periodicity of about 13 nm. In addition to the original (primary) Dirac points, the moiré superlattice produces new (secondary) superlattice Dirac points, located at a different energy (*34*). Those two have different velocities and energy gaps: at ambient pressure, $v = 0.94 \times 10^6$ m/s and $2\Delta = 30$ meV for the original Dirac point, and $v = 0.5 \times 10^6$ m/s and $2\Delta = 20$ meV for the superlattice Dirac points (*35, 37*). The size of the gap depends on the superlattice periodicity and it could be enhanced by interaction (*61*). We note that even at the original Dirac point, the velocity is slightly modified. We consider the original Dirac points instead of the superlattice Dirac points. The latter have the valley degeneracy of six and anisotropic Dirac cones whereas the valley degeneracy of the former is two.

The scattering time is estimated from a transport measurement with a high-quality sample (*48*). At 300 K, they observed the mobility $\mu \approx 90{,}000\,\mathrm{cm}^2/(\mathrm{V\,s})$ with the carrier density $n = 1 \times 10^{12}\,\mathrm{cm}^{-2}$, which amounts to the scattering time $\tau \approx 1.13\,\mathrm{ps}$. The corresponding frequency is $(2\pi\tau)^{-1} \approx 141\,\mathrm{GHz}$ and the mean free path is $\ell \sim v_F\tau \approx 1.6\,\mu\mathrm{m}$. We note that the Fermi wavelength at $n = 0.5 \times 10^{12}\,\mathrm{cm}^{-2}$ is $\lambda_F \approx 0.05\,\mu\mathrm{m}$, which is still shorter than the mean free path: $\lambda_F \ll \ell$. To estimate the impurity strength, we need to know the impurity concentration. From transport and scanning tunneling microscopy/spectroscopy (*47, 49*), we approximate the impurity density as $n_i \approx 1{\times}10^9\,\mathrm{cm}^{-2}$, which results in $V_i \approx 2.77{\times}10^{-13}\,\mathrm{eV\,cm}^2$ ($nV_i \approx 277\,\mathrm{meV}$ at $n = 1 \times 10^{12}\,\mathrm{cm}^{-2}$). Since the velocity is only slightly modified from the value without a superlattice structure, we employ the value $\lambda/v = a/4$ obtained from a tight-binding model, where a is the carbon atom spacing, given by $a = 1.42\,\text{Å}$ (*40, 41*). Those values yields the ratio $\tau/\tilde{\tau} \approx 0.003$ at $n = 1{\times}10^{12}\,\mathrm{cm}^{-2}$. In the present calculations, we do not consider the temperature dependence of the parameters or the origin of scattering and inhomogeneity of samples for simplicity, although the scattering time becomes longer in lower temperatures.

For bilayer graphene, high-quality bilayer graphene grown by chemical vapor deposition (CVD) and detached on hBN realizes the mobility $\mu = 30{,}000\,\mathrm{cm}^2/(\mathrm{V\,s})$ at 300 K (*51*). An out-of-plane electric field (displacement field) D opens a band gap of about $2\Delta = 100\,\mathrm{meV}$ with $D \approx 1.1\,\mathrm{V/nm}$ (*50*). The coefficient $\lambda = (2m)^{-1}$ is determined by the effective mass $m \approx 0.033m_e$ (m_e: electron mass) and $v \approx 1 \times 10^5\,\mathrm{m/s}$ (*52, 53*). Evaluating at $n = 1 \times 10^{12}\,\mathrm{cm}^{-2}$, we find the scattering time $\tau \approx 0.96\,\mathrm{ps}$, corresponding to the frequency $(2\pi\tau)^{-1} \approx 166\,\mathrm{GHz}$, and the mean free path $\ell \sim v_F\tau \approx 0.35\,\mu\mathrm{m}$. We assume the impurity concentration $n_i \approx 1 \times 10^9\,\mathrm{cm}^{-2}$, considering its high mobility, to obtain the impurity strength $V_i \approx 1.06 \times 10^{-13}\,\mathrm{eV\,cm}^2$ ($nV_i \approx 106\,\mathrm{meV}$ at $n = 1 \times 10^{12}\,\mathrm{cm}^{-2}$). At the carrier density $n = 1 \times 10^{12}\,\mathrm{cm}^{-2}$, we have the ratio $\tau/\tilde{\tau} \approx 0.018$.

The carrier density dependence of ϵ_F, v_F, and $\sigma(0)$ is shown in Fig. S2, and the frequency

dependence of σ, χ, η_I, and η_I is depicted in Fig. S3. The frequency and temperature dependence of the response are given in Figs. S4 and S5. We note that the scattering times used for the calculations are those at 300 K. The scattering time becomes longer in lower temperature, which makes the linear conductivity σ, the second-order conductivity χ, and the reduced current responsivity η_I larger, whereas the low- and high-frequency values of the reduced voltage responsivity η_V barely change.

Section S5. Surface state of a topological insulator

A surface state of a topological insulator also lacks inversion and thus hosts the rectification effect (*18*). Here we take an example of the surface state of the topological insulator Bi_2Te_3 (*18, 62*), where the Hamiltonian is

$$H(\boldsymbol{k}) = v(k_x\sigma_y - k_y\sigma_x) + \frac{\lambda}{2}(k_+^3 + k_-^3)\sigma_z \tag{S112}$$

leading to the energy spectrum

$$\epsilon_{\boldsymbol{k}} = \sqrt{v^2k^2 + \lambda^2k^6\cos^2 3\theta} \tag{S113}$$

The origin $\boldsymbol{k} = 0$ is located at Γ point and the k_x axis is parallel to ΓK line. Unlike the previous two cases based on graphene, it has a single Dirac spectrum centered at Γ point. Furthermore, the topology of the wavefunction in the bulk prohibits a mass gap of the surface states. In this case, a surface breaks inversion by itself and the symmetry is C_{3v}.

For the present Hamiltonian, short-ranged impurities without momentum dependence do not produce finite $w^{(A)}$, nor does the second-order response. This issue can be circumvented instead by considering Coulomb impurities, where the impurity potential is inversely proportional to the distance from the impurity position: $V(\boldsymbol{r}) \propto \sum_j |\boldsymbol{r} - \boldsymbol{r}_j|^{-1}$. Assuming that the hexagonal warping of the Fermi surface is small, we have the matrix element of the Coulomb impurity

potential on the Fermi surface as

$$V_{\boldsymbol{k}\boldsymbol{k}'} = \frac{V_c}{\left|\sin\left(\dfrac{\theta-\theta'}{2}\right)\right|} \tag{S114}$$

Then, we obtain the scattering rates

$$w^{(S)}_{\boldsymbol{k}\boldsymbol{k}'} = \frac{2\pi n_i V_c^2}{\tan^2\left(\dfrac{\theta-\theta'}{2}\right)}\delta(\epsilon_{\boldsymbol{k}} - \epsilon_{\boldsymbol{k}'}) \tag{S115}$$

$$w^{(A)}_{\boldsymbol{k}\boldsymbol{k}'} \approx \frac{8\pi n_i V_c^3 \epsilon_F^3}{v^5}\lambda c_1 \operatorname{sgn}\left[\sin\left(\frac{\theta-\theta'}{2}\right)\right]\cos\left(\frac{\theta-\theta'}{2}\right)(\cos 3\theta - \cos 3\theta')\delta(\epsilon_{\boldsymbol{k}} - \epsilon_{\boldsymbol{k}'}) \tag{S116}$$

with the numerical factor $c_1 \approx 0.93$ obtained from the numerical integration over momenta.

Since there is a single Fermi surface and time-reversal symmetry relates the Fermi surface with itself, $\chi^{(0)}$ vanishes with the single Fermi surface. A finite second-order conductivity can be found in $\chi^{(1)}$ as follows

$$\chi^{(1)}_{xxy} = \chi^{(1)}_{xyx} = \chi^{(1)}_{yxx} = -\chi^{(1)}_{yyy} \approx e^3 \nu \frac{\tau^3}{\tilde{\tau}} \operatorname{Re}\left[\frac{c_1}{1-i\omega\tau} + \frac{c_2}{(1-i\omega\tau)^2}\right] \tag{S117}$$

Here, we assume for simplicity the constant scattering time $\tau \approx (2\pi D_0 n_i V_c^2)^{-1}$ obtained from $w^{(S)}$, and the scattering time originated from $w^{(A)}$ is defined by

$$\tilde{\tau}^{-1} = \lambda \frac{2 n_i V_c^3 \epsilon_F^4}{\pi v^7} \tag{S118}$$

The two numerical factors $c_1 \approx 0.87$ and $c_2 \approx 0.14$ are evaluated by numerical integrations.

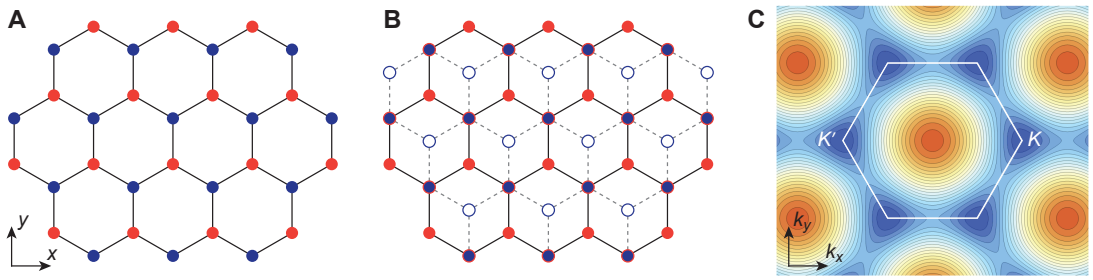

Fig. S1. Monolayer and bilayer graphene models. (**A**) Lattice structures of monolayer graphene and (**B**) bilayer graphene along with the crystal axes. The red and blue circles depict distinct sublattice sites with different potential energies, and the filled and empty circles correspond to atoms on different layers. Both lattices have reflection planes parallel to the y axis and its symmetry partners under the three-fold rotation. (**C**) Brillouin zone and energy contours for the monolayer model. With small doping, there are trigonally-warped Fermi surfaces around K and K' points, facing the opposite directions. The bilayer model exhibits the similar Fermi surfaces as the monolayer ones.

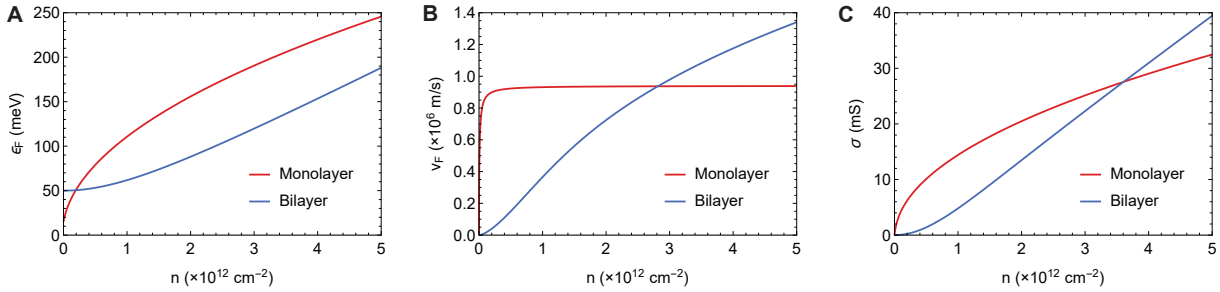

Fig. S2. Carrier density dependence of the material properties. (**A**) Fermi energy ϵ_F, (**B**) Fermi velocity v_F, and (**C**) linear DC conductivity σ at zero temperature. Refer to Sec. 4 for the values of the parameters.

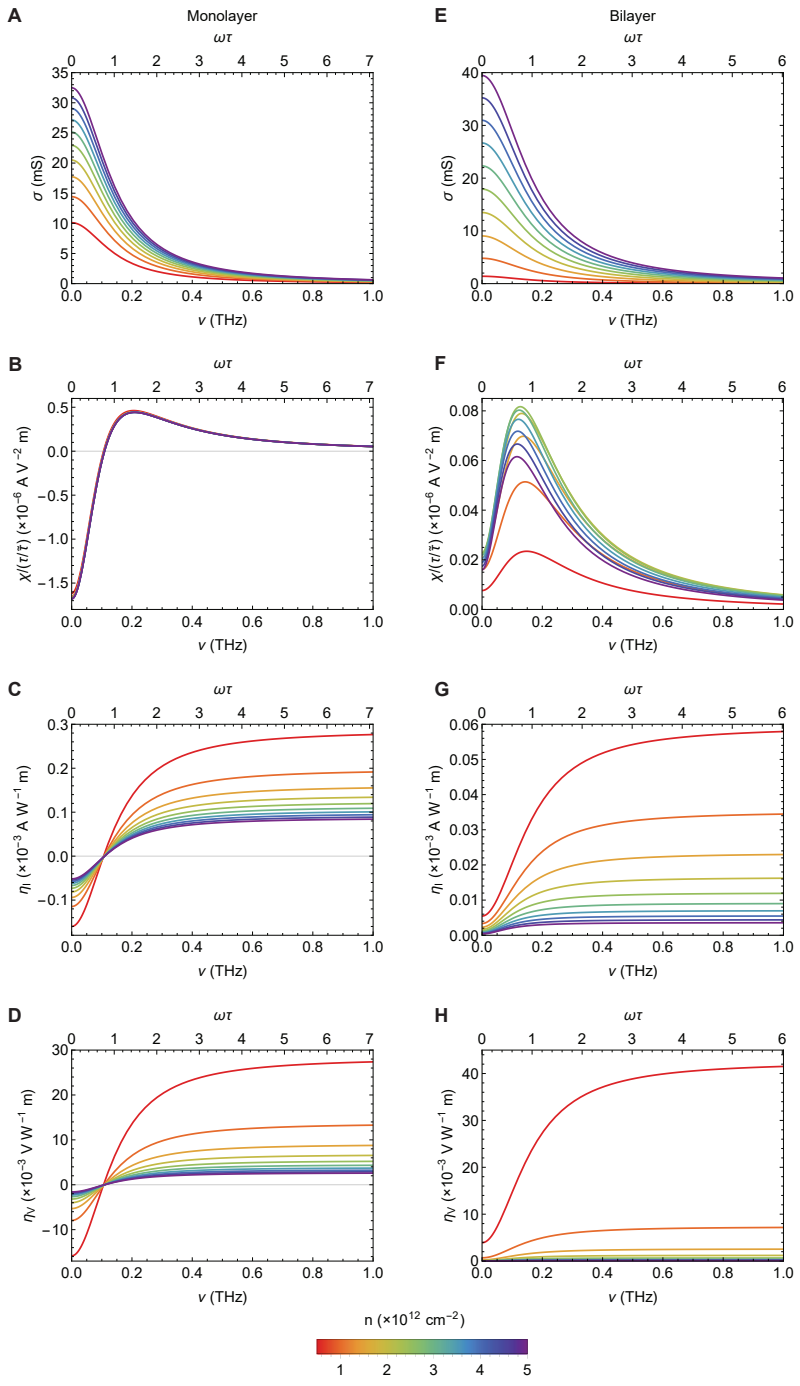

Fig. S3. Frequency dependence of the response. (**A** and **D**) Linear conductivity σ, (**B** and **F**) second-order conductivity χ, (**C** and **G**) reduced current responsivity η_I, and (**D** and **H**) reduced voltage responsivity η_V. Panels (A) to (D) correspond to the monolayer model, and (E) to (H) correspond to the bilayer model. The carrier density is changed from $0.5 \times 10^{12}\,\mathrm{cm}^{-2}$ (red) to $5 \times 10^{12}\,\mathrm{cm}^{-2}$ (purple), and the temperature is set to be zero. Refer to Sec. 4 for the values of the parameters.

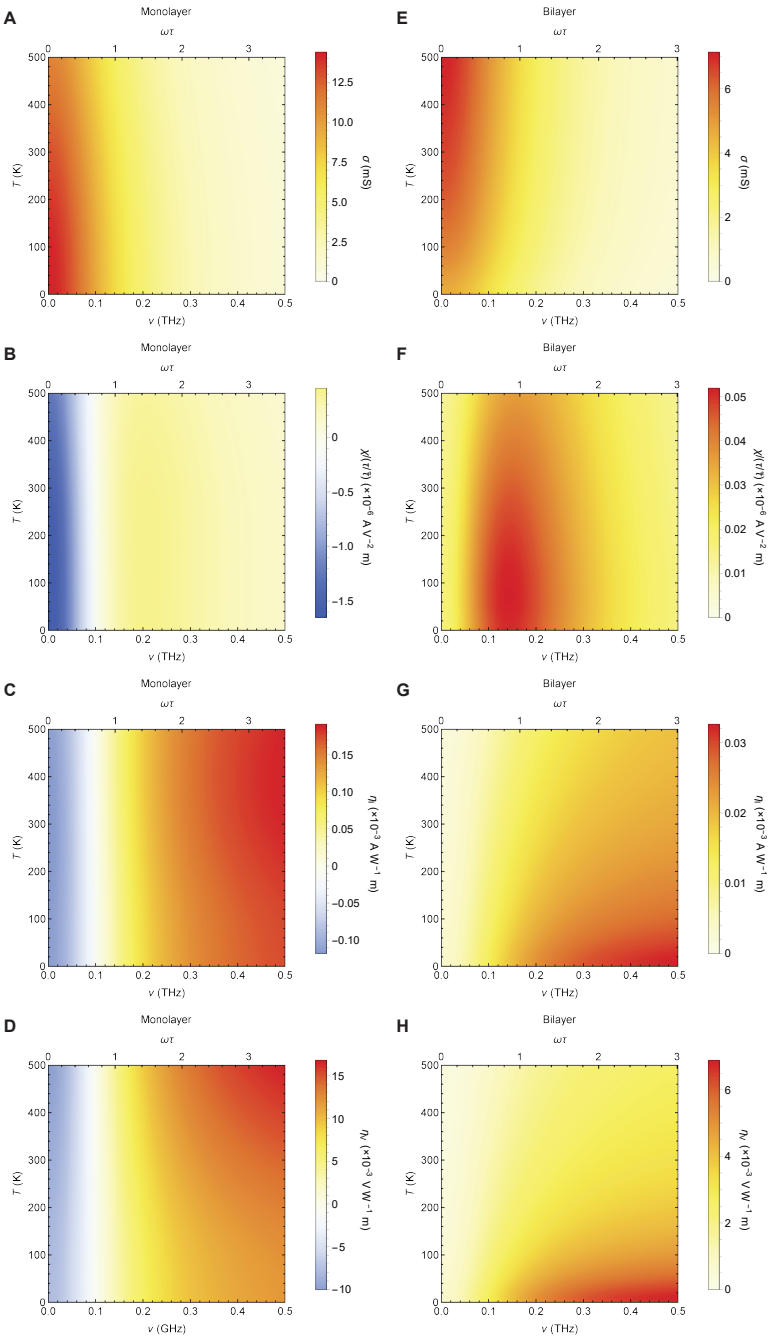

Fig. S4. Frequency and temperature dependence of the response. (**A** and **E**) Linear conductivity σ, (**B** and **F**) second-order conductivity χ, (**C** and **G**) reduced current responsivity η_I, and (**D** and **H**) reduced voltage responsivity η_V. The carrier density is fixed at $n = 1 \times 10^{12}\,\mathrm{cm}^{-2}$.Panels (A) to (D) correspond to the monolayer model, and (E) to (H) correspond to the bilayer model. We assume that the scattering time τ is constant independent of temperature; see Sec. 4 for the values of parameters.

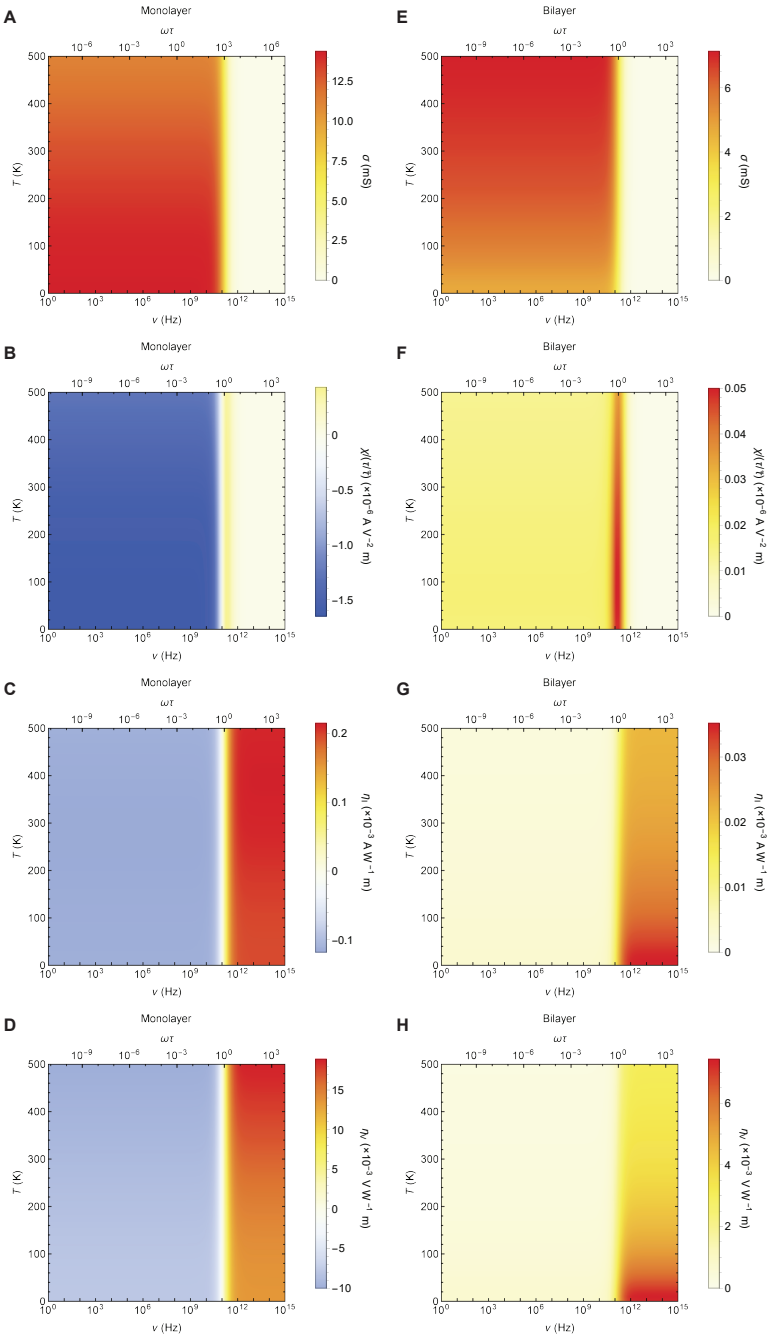

Fig. S5. Frequency and temperature dependence of the response with a logarithmic scale for the frequency axis. (**A** and **E**) Linear conductivity σ, (**B** and **F**) second-order conductivity χ, (**C** and **G**) reduced current responsivity η_I, and (**D** and **H**) reduced voltage responsivity η_V. The same results as Fig. S4 are plotted with the frequency in a logarithmic scale.